Nanoscale modification of silicon surfaces via Coulomb explosion

Hai-Ping Cheng

Department of Physics & QTP, University of Florida, Gainesville, Florida 32611

J. D. Gillaspy

Physics Laboratory, National Institute of Standards and Technology, Gaithersburg, Maryland 20899

Coulomb explosions on silicon surfaces are studied using large-scale molecular-dynamics simulations. Processes under investigation begin by embedding a region consisting of 265–365 singly charged Si^+ ions on a Si [111] surface. The repulsive electrostatic energy, initially stored in the charged region, leads to a local state with ultrahigh pressure and stress. During the relaxation process, part of the potential energy propagates into the surrounding region while the remainder is converted to kinetic energy, resulting in a Coulomb explosion. Within less than 1.0 ps, a nanometer-sized hole on the surface is formed. A full analysis of the density, temperature, pressure, and energy distribution as functions of time reveals the time evolution of physical properties of the systems related to the violent explosive event. A shock wave that propagates in the substrate is formed during the first stage of the explosion, $0 < t < 100$ fs. The speed of the shock wave is twice the average speed of sound. After the initial shock the extreme nonequilibrium conditions leads to ultrarapid evaporation of Si atoms from the surface. Qualitatively similar features are observed on a smaller scale when the number of initial surface charges is reduced to 100. Our simulations demonstrate the details of a process that can lead to permanent structure on a semiconductor surface at the nanoscale level. The work reported here provides physical insights for experimental investigations of the effects of slow, highly charged ions ($Q > 40$, e.g.) on semiconductor materials. [S0163-1829(97)02104-8]

I. INTRODUCTION

Fabricating structures at the nanometer length scale has become an increasingly active area for physical, chemical, and material sciences.[1,6] Various experimental techniques, from the assembly of nanosized clusters and chemical etching to ion beam lithography and surface sputtering, have been developed to construct nanostructured materials.[7–14] These and other advances in nanotechnology have created opportunities for contemporary scientific investigations of the physical properties of novel materials and the transient states and processes of physical systems. Many physical phenomena that occur in the nanometer regime and femtosecond to picosecond time domain exist under extreme physical conditions. Much research effort has been focused on the physical mechanisms underlying material properties and nanomachining.[15–19] Understanding the physical origins of the observed phenomena, the time evolution of thermodynamical properties of systems far away from equilibrium, and the relationships among physical properties, intermediate states in the physical processes, and the ultrafine structure of materials is of basic and technological importance.

Accompanying the technological achievements, scientists have been seeking new theories to explain the results observed in nanoscale experiments. Much attention has been given to the development of new methodology for theoretical studies. The necessity for new methods arises for several reasons. First, traditional condensed matter approaches can not be applied directly to nanostructured systems because of surface or boundary effects. Second, traditional statistical theories are not suited for solving problems associated with states far from equilibrium. Third, traditional atomic and molecular theories fail to predict the behavior of nanoscale systems due to the large number of degrees of freedom in these systems.

Advances in computer science and technology have exerted a significant influence on scientific research in the area of nanoscale science. Large-scale computer simulations are becoming powerful tools for investigations of complex physical and chemical processes.[20–23] By deriving physical quantities such as kinetic energy, potential energy, pressure, and temperature from the trajectories of atoms in phase phase, simulations can correlate microscopic pictures with macroscopic phenomena. Time-dependent simulations of molecular dynamics allow studies of physical and chemical properties as functions of time. Results from the simulations can often be compared directly to the experimental measurements, and can also be used as input for analytical theoretical modeling.[15] Consequently, innovative ideas such as directing chemical reaction pathways,[24,25] controlling cluster-surface collision outcomes,[15] preparing, size selecting, and identifying nanocrystals[7] become well understood realities in the laboratory after iterations in the cycle of simulation, modeling, and experimentation.

II. EXPERIMENTAL BACKGROUND

The goals of our investigations are to search for new methods for nanofabricating of semiconductor surfaces and to study characteristic features of the phenomena involved in these processes. We are especially encouraged by the recent progress in the electron beam ion trap[14,26–30] (EBIT) experiments. In these experiments, the projectile atoms are highly ionized ($Q > 40+$ typically), and impinge on the target sur-

face with low kinetic energy. Unlike high kinetic energy particle-surface sputtering experiments, the key issue in the EBIT experiments is the internal electrostatic potential energy of the ions. This internal energy can be over 750 keV, five orders of magnitude higher than that for a conventional (singly charged) ion. When a single such highly charged ion neutralizes itself by impacting a solid, it can create a surface structure of order 10 nm in dimension. The size of the structure can be varied by adjusting the charge of the incident ion,[26,31] and the efficiency of the feature formation is essentially 100% (one feature for each incident ion). Speculations emerging from experimental evidence suggest that there may be technological applications of the highly charged ions as a new method for modifying or etching semiconductor or insulator surfaces.[26,30–36] However, there is very little information about the Coulomb explosion process, which is proposed to be the main cause for surface damage.[26,37] In fact, it is only recently that clear evidence for the existence of surface Coulomb explosions induced by slow highly charged ions has been obtained.[38,27] In this paper, we report the results of computer simulations of Coulomb explosions on silicon surfaces. These simulations are performed in conjunction with ongoing experimental studies of highly charged high Z ion-surface bombardment at NIST.[30]

III. MODELING AND SIMULATIONS

The basic physical picture leading to a Coulomb explosion in a surface is as follows. As a highly charged ion approaches a surface, its intense Coulomb field is sufficient to rapidly pull electrons from the solid, even when the ion is still many atomic diameters away from the surface (e.g., up to 540 Bohr radii, in one model[39]). Electrons are captured into high-lying Rydberg levels, producing a superexcited ''hollow atom,'' which may be fully neutralized.[40–43,35] The atom can decay (collapse) towards its ground state via Auger cascade, ejecting electrons in the process,[26,34] or by other mechanisms such as radiative decay or surface plasmon formation.[45] Only if electrons are ejected fast enough and the ion approaches the surface slowly enough can electrons continue to be removed from the solid during the ion's approach. A fully stripped incident ion of atomic number Z can therefore remove at least Z electrons, perhaps quite a few more, during its approach. If the ion is not fully neutralized and collapsed prior to impact, more electrons can be removed during and after the collision with the surface. Observations exist for incident charges up to Th^{75+} ($Z=90$) where approximately 300 ejected (free) electrons per ion were detected,[26,44] not including the additional $Q=75$ electrons that were removed simply to neutralize the incident ion. Theories predict that by increasing the charge of the incident ion even further it should be possible to remove over 1000 electrons per ion.[46] Earlier scaling-law extrapolations from low-charge data had indicated that this number might be several times larger still.[46] If even a fraction of these electrons are removed sufficiently fast that the solid cannot replenish them, a localized region of the surface will become charged. Data on GaAs indeed show that the replenishment of electrons from the surrounding solid to the locally charged region does not proceed fast enough to circumvent the effect that we discuss here.[36] As we will show, the localized

charged region overcomes the cohesive forces that hold the solid together, and the region explodes under its mutual electrostatic repulsion. Subsequent shock waves and thermal processes ensue, leaving a crater-like feature in the surface. To our knowledge, the work reported here is the first full-scale three-dimensional molecular dynamics calculation for the Coulomb explosion of a surface. Earlier work on the problem was restricted to two dimensions, and carried out for 50 times fewer atoms than we consider here.[4]

The simulations begin by preparing a Si [111] surface in its ground state. The sample consists of 34 560 atoms distributed over 24 layers. Thus, the thickness of the surface is approximately 40 Å (70 a.u.), and the width and length are about 140 Å. Periodic boundary conditions are applied only to the substrate in the x and y directions but not to the ions. This ensures that there are no artificial long-range Coulomb interactions existing between neighboring unit cells. Our results are checked for artifacts by performing additional simulations with different sample sizes. In order to stabilize the surface, 6 layers of static atoms are placed at the bottom. The remaining 18 layers, above the static layers, are dynamical. Temperature control is applied only to the deepest dynamical layer. This method of applying temperature control leads to a realistic simulation of atomic motion during a dynamic event. At the same time, it allows energy exchange between the system and a constant temperature heat bath.

At $t=0$, 265–365 atoms in a hemispherical region in the center of the surface are singly charged. This initial conditions is chosen to imitate the consequences of bringing a slow, high-charged ion, such as Xe^{+44} or U^{+92} into the neighborhood of a nonmetal surface. Such an initial condition has been put forth by a number of researchers active in this field,[33,35,38,36] but to our knowledge this is the first time that the subsequent Coulomb explosion has been investigated at the atomic level by detailed simulations and calculations rather than simply depicted as an artist's conception. Since there is some evidence that the time scale for the electron emission from a surface can be very short,[26,34,40,48,44] we separate the dynamics of the surface explosion from the process of multielectron capture and Auger cascade, which leads to the initial conditions assumed here. This simplified model is supported by the evidence of fast Coster-Kronig transitions in ion-silicon surface interactions.[34] Here, we focus on the dynamics of the surface atoms after a huge amount of repulsive electrostatic energy is suddenly deposited. The number of ions is chosen to be either 365 or 265. This is consistent with experimental results,[26] in which the number of electrons removed from the surface is found to be more than 4 times the charge number of the slow (v_i is of order 10^3 m/s) incoming ion.

Each silicon atom interacts with the other atoms via a three-body Tersoff potential function,[49] which has been tested for both crystalline and amorphous silicon. The Si^+ ions interact simply via pairwise Coulomb repulsion. In order to describe interactions between Si and Si^+, we combine information from experimental measurements and first-principles calculations[50] on Si-Si and Si- Si^+ dimers. These data are then fitted to a function,

$$V(r_{ij}) = \varepsilon \left[\left(\frac{\sigma}{r_{ij}} \right)^{12} - \left(\frac{\sigma}{r_{ij}} \right)^4 \right]. \tag{1}$$

The term $1/r^4$ is chosen due to the interaction of the charge (on Si^+) and the induced dipole (on Si). The parameters σ and ε are chosen to be 3.69 a_0 and 9.17 eV, respectively. It should be pointed out that the Si-Si^+ and Si^+-Si^+ potentials used in our simulations are not extensively optimized. However, for the events of interest here, they capture the basic physical features of the important atomic interactions, and provide sufficient numerical accuracy as well.

The equations of motion for each particle in the dynamical substrate are then integrated using Gear's predictor-corrector algorithm.[51] The time step of $\Delta t = 0.4$ fs is chosen to maintain energy conservation. The temperature of the bottom dynamical layer is controlled to be 300 K. The systems evolve in time according to classical Newtonian dynamics. Positions, velocities, and accelerations of all the atoms and ions are obtained via numerical solution of the classical equations of motion at each time step.

IV. RESULTS

Figure 1 shows several snapshots of a system with 365 ions, at $t = 0.0$, 40.0, 80.0, and 360.0 fs. We see that the region filled with ions expands significantly at $t = 40$ fs, and a hole is formed by 80 fs. At this point, the size of the hole is similar to the size of the initially charged region. The last snapshot displays a much larger hole with many Si atoms, as well as Si^+ ions, exploding from the surface. More atoms and ions leave the surface as the simulation continues. We separate the process into two stages. First is the initial, extremely violent explosive stage, which ends at 80–100 fs. This is followed by a period of rapid, high-temperature evaporation. The detailed dynamics of these stages can be analyzed by studying various physical properties, such as pressure, energy, density, and temperature.

Figure 2 depicts the temperature of several subdivisions in the substrate as a function of time. These subdivisions are three-dimensional concentric shells that coincide with the center of the hemispherical charged region. The thickness of each shell is chosen to be 2.6 Å (5 a.u.). The innermost shell is just outside the initially charged region. Panel (a) shows the results for a 365-ion system: the temperature of each shell increases sharply at a rate of over 10^{18} K/s, peaks at over 10^5 K, and then begins to relax back towards ambient temperature. Two striking phenomena can be observed in this picture. First is the time delay for two adjacent shells to undergo the sudden temperature jump. This is a signature of shock-wave propagation. The speed of the wave is estimated to be 2.0×10^4 m/s, or a little more than 2 times the average speed of sound in silicon.[52] The rapid dissipation of the shock wave at about 80–100 fs coincides with the time required for the charged region to expand significantly and lose its geometric symmetry. Second, we note that the rate of temperature increase observed here is extremely fast. Compared with other methods used for rapid heating, for example, by laser heating[53,54] or cluster-surface collision,[15] 10^{18} K/s is several orders of magnitude faster. Even if we factor out the initial impact of the shock wave, the temperature at 100 fs is above 6000 K, corresponding to an average rate of about 10^{17} K/s. After 100 fs the temperature begins to decrease, as Si atoms are ejected from the surface. Panel (b) shows the same quantities for a system starting with 265

ions. Again, we observe a pattern very similar to that in panel (a). The time for the shock wave to collapse also coincides with that in (a). The only noticeable difference is the temperature. The order of the magnitude of the heating rate, however, remains the same.

The initial energy in the charged region is calculated to be 87.3 keV (3.21×10^3 a.u.) due to the Coulomb repulsive interaction of 365 ions. For 265 ions, the initial energy is 50.8 keV (1.87×10^3 a.u.). Figure 3 shows the three curves representing the kinetic energy (solid line), potential energy (dashed line), and energy propagating to the substrate (dotted line). For $t < 100$ fs, the amount of potential energy converted to the kinetic energy of the ions is greater than the energy transfer to the substrate. The two curves cross each other at 95 fs in both panels (a) and (b). At the crossing point, the total kinetic energy of the ions is slightly less than 10^3 a.u. for 365 ions, and 580 a.u. for 265 ions. We estimate that these numbers correspond to 31% of the initial potential energy. After 100 fs the rate of increase of the kinetic energy of the ions slows significantly. The crossing time of the two energy curves coincides with the ending of the propagation of the shock wave. Somewhat later, at 110–120 fs, the potential energy drops below the other two energy curves.

In Fig. 4, snapshots of the pressure and potential energy distributions (for 365 ions) at several times are shown. At $t = 0$, the large amount of repulsive Coulomb energy stored in the charged region causes an extremely high pressure in the hemispherical region. The highest pressure in the system corresponds to 1.4×10^3 GPa of pressure. However, the value of highest pressure quickly drops to 4.3×10^2 GPa at $t = 40$ fs, and then to 1.8×10^2 GPa at $t = 80$ fs. At $t = 360$ fs, the pressure is still very high, about 9.2 GPa, even though it is much smaller than its initial value. The potential energy distribution undergoes a similar evolution, where the highest-energy value for $t = 0$, 8, 16, 40, and 80 fs is 11.0, 10.7, 9.9, 7.3, and 5.2 a.u., respectively. This value further decreases to 1.5 a.u. at 360 fs. Note that the pressure decreases faster than the energy during the expansion, due to the relation $P \propto (\partial E / \partial V)$.

Density distributions (for the 365 ions system) at different time instants are displayed in Fig. 5. At $t = 0$, the distribution is uniform throughout the substrate as expected (not shown). The density of the charged region decreases rapidly, in contrast with the formation of a high density ring near the center region. The highest density found in the explosion, which occurs between 40 and 55 fs, reaches more than 50% of the initial density, thus indicating an extremely nonequilibrium environment. A hole of 35.3 Å in diameter and 13.8 Å in depth is quickly formed at the center of the surface. This initial phase (at $t < 100$ fs) of the hole formation is mainly due to Coulomb explosion. A total number of 141 particles, including 115 ions and 26 atoms, are ejected from the surface. At $t < 100$ fs, the large amount of energy that is delivered into the substrate melts the silicon crystal. Eventually, atoms with sufficient kinetic energy evaporate from the surface. At $t = 360$ fs, the size of the hole is about 62.5 Å in diameter and 19.6 Å in depth. A total number of 768 particles, including 598 atoms and 170 ions, have left the surface. The diameter of the hole further increases to more than 10 nm at about 600 fs.
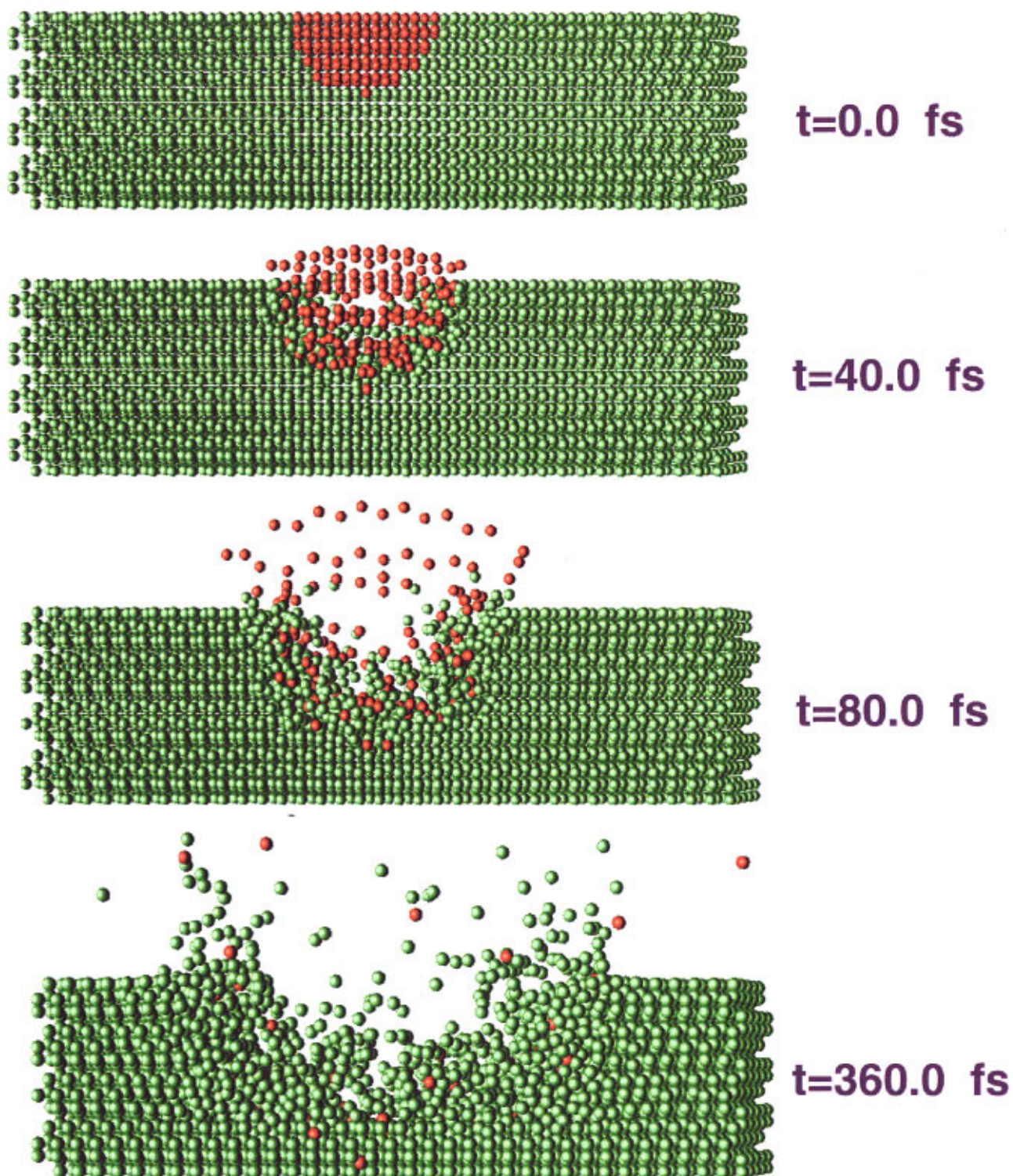
FIG. 1. (Color) Snapshot of the time evolution of the Coulomb explosion process. Red and green spheres are used to indicate Si$^+$ ions and Si atoms, respectively. This particular system consists of 365 ions. The initial Coulomb repulsive energy stored in the hemispherical region is about 87.3 keV. Between $t=0$ and 40 fs, the charged region expands significantly. At $t=80$ fs, over 100 ions are ejected from the surface, forming a pronounced hole. By 360 fs, the hole is much larger, and about 800 atoms and ions are driven from the surface.

Figure 5 also shows the temperature distributions at several times. The temperature of hottest spot in the system is 7.1×10^4, 2.5×10^5, 9.2×10^5, and 1.6×10^6 K for $t=8$, 16, 40, and 80 fs, respectively. We note that the temperature is derived from the total kinetic energy of the ions. As can be seen in the figures, the system is far from equilibrium. Even after the initial shock wave passes, the temperature gradient is very large in the substrate. This extremely nonequilibrium situation is directly responsible for the rapid evaporation of the atoms.
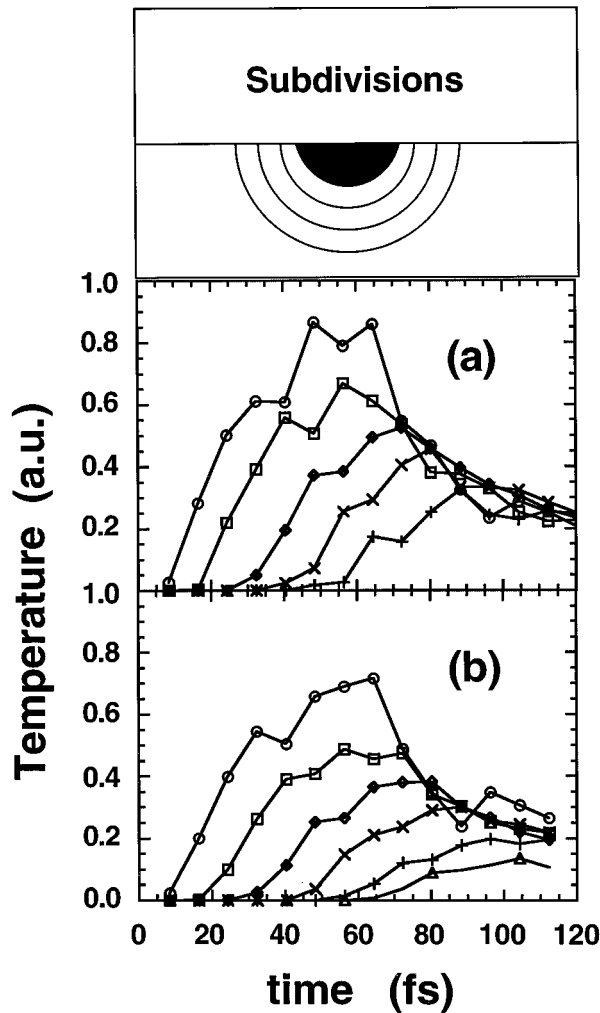
FIG. 2. Temperature of subregions of the substrate as functions of time. Panel (a) is the plot of a system consisting initially of 365 Si$^+$ ions, and panel (b) is for 265 Si$^+$ ions. The subregions correspond to several concentric shells with a thickness of 5 a.u. The jumps in temperature seen in each shell indicate a shock wave propagating through the substrate. The patterns in panels (a) and (b) are very similar. After 100 fs, the temperatures in different shells converge to the same value. Numbers are given in a.u. where 9.50×10^{-4} a.u.=300 K.

V. DISCUSSION

The results of our simulations are in rough agreement with experiments. The fact that the crater does not preserve the hemispherical shape of the initial conditions but instead becomes more oblate may be partly an artifact due to the finite number of layers used in the simulation. Results from simulations with only 100 ions in the initially charged region show crater formation of a similar type, but with a more spherical shape. If the crater shape shown in Fig. 5 is convolved with a typical atomic force microscope (AFM) tip radius of 30 nm the *apparent* (measured) depth would be only 0.4 nm for a 10-nm-diameter crater. A more spherical crater of the same diameter would appear to have roughly the same apparent depth, so the distinction between actual depths would not show up in existing experiments. Craters in mica have been observed to have apparent depths of 0.3 nm
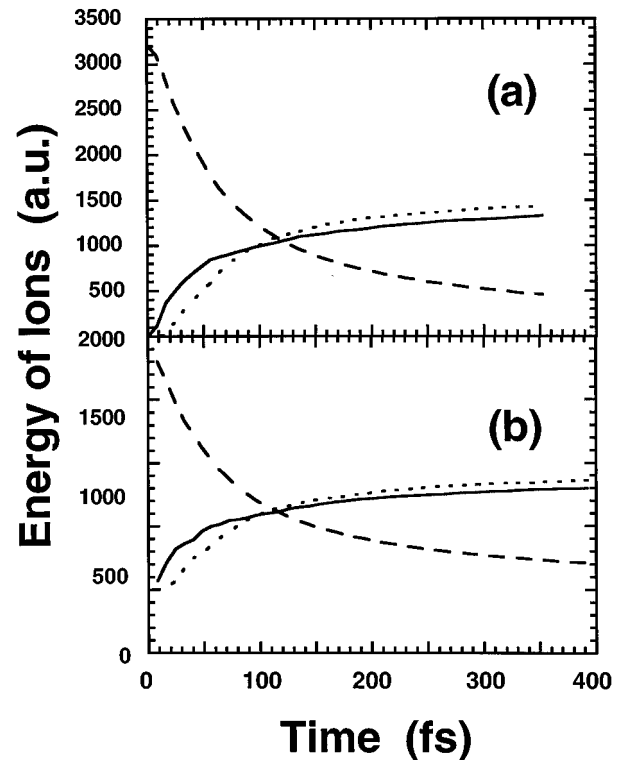

FIG. 3. Kinetic energy (solid line) and potential energy (dashed line) of the ions during the Coulomb explosion. The dotted line is the energy transferred from the ions to the substrate. Panel (a) is for the 365-ion system and panel (b) the 265-ion system. Notice that after the initial shock, which ends at 80–100 fs, most of the energy originally stored in the ions is transferred to the substrate. After this time, the potential energy decreases more slowly than at the beginning. At the same time, the gain in kinetic energy of the ions slows down significantly compared to that during the initial 80 fs. Panels (a) and (b) display similar patterns. The energies are plotted in a.u. where 1 a.u.=27.2 eV.

and diameters of 7 nm,[55] both of which scale up with increasing charge of incident the ion.[26,33] As of yet, there are no published data showing crater topography in silicon under the influence of highly charged ion bombardment. Such data would be of great theoretical and practical interest. The question of whether there is a critical range of electrical conductivity above which Coulomb explosions are quenched by the ability of free carriers to flow quickly into the region being charged by the incident ion might be addressed by varying the initial temperature and doping of the silicon. By using cryogenic temperatures and highly doped silicon, the full range of possibilities from perfect insulator to semimetals can be probed in one system.

We emphasized that this simulation does not address the question of whether or not surface Coulomb explosions exist (or can be made to) in the laboratory. It only helps elucidate how the process would unfold and what the aftereffects would be if the assumed initial condition could be realized. Together with the explosion time scales determined in this work, a number of atomic physics and materials time scales must also be considered in order to predict what conditions need to be achieved in the laboratory in order to produce the Coulomb explosion.[56-60,43,36] This will be the topic of a more
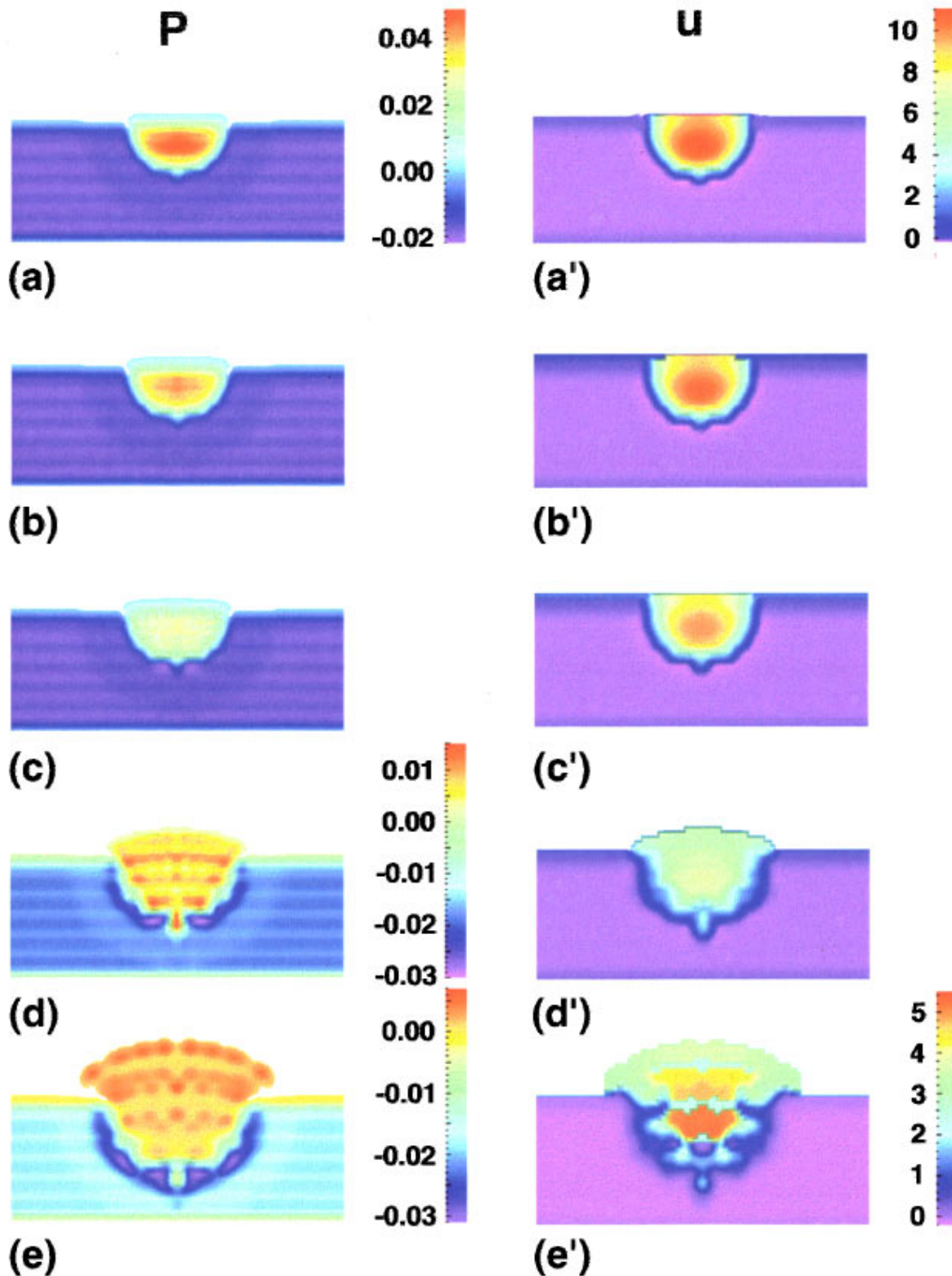
FIG. 4. (Color) Spatial distributions of pressures (left column) and potential energy (right column) for the system with 365 ions, at several time instants. The times represented in panels (a)–(e) and (a')–(e') are 0, 8, 16, 40, and 80 fs, respectively. All units are in a.u., where 1 a.u.$= 2.94\times10^{13}$ Pa or 2.94×10^{4} GPa in pressure. The same color scales are used in (a)–(c) and (a')–(d') to demonstrate the dissipation between 0 and 16 fs. Different color scales for (d), (e), and (e') are used to focus on the detail of the patterns in the plots.

complete analysis once both upper and lower bounds on all the relevant time scales become better known. Recent experiments have yielded evidence that the necessary conditions may already have been achieved in two instances.[26,36]

We would also like to stress the fact that we consider this simulation to be only a first step towards a more detailed understanding of the Coulomb explosion process. The present simulations focus mainly on effects derived from
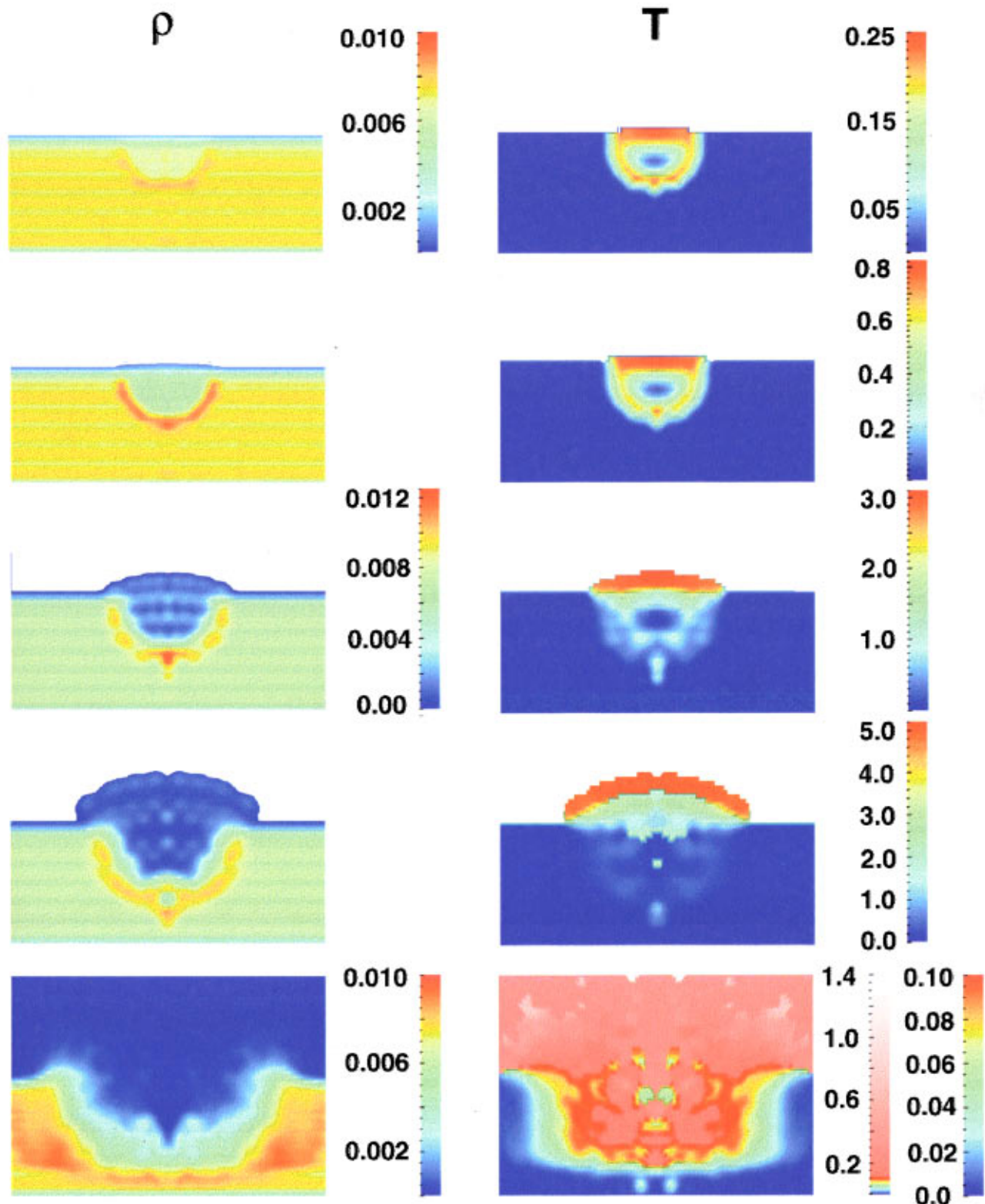
FIG. 5. (Color) Spatial distributions density (left column) and temperature (right column) for the system with 365 ions, shown at several time instants. The times represented in panels (a)–(e) and (a′)–(e′) are 8, 16, 40, 80, and 360 fs. All units are in a.u., where 1 a.u.=6.75 $\times 10^{30}$ m^{-3} or 6.75$\times 10^{24}$ cm^{-3} in density. The same color scales are used in (a) and (b) and (c) and (d) to demonstrate the density changes between 8 and 40 fs. A different color scale is used for (e) to display the hole on the surface at 360 fs. For the right column, each picture has a different color scale due to the rapid changes in kinetic energy. Panels (a′)–(d′) show the hot leading edge of the ions during the explosion. For (e′) two color scales are used to show both the extremely hot region and the details of the temperature distribution in the substrate. Deep blue to deep red describes $0<T<0.1$ a.u. (or, $0<T<3\times 10^4$ K), and deep red-pink-white describes $0.1<T<1.4$ a.u., where 1.4 a.u.=4.4$\times 10^6$ K.

stored potential energy. In the case of ion-surface bombardments in which the kinetic energy of the incident ion is comparable to or greater than the potential energy, the effects of the ion colliding on the surface should be considered. Experimental evidence with highly charged ions on mica, however, shows that crater topography is essentially independent of the kinetic-energy–potential-energy ratio (R) for R $= 0.08$– 18 (kinetic energy from 4.4–440 keV.[55] Studies on GaAs with singly charged ions having kinetic energy comparable to that of the slowest highly charged ions have shown craters that consist of only one or a few ejected atoms.[6] These craters are so small that they have only been observed with UHV-STM (ultrahigh vacuum scanning tunneling microscope) techniques, and they would therefore be invisible in all of the highly charged ion studies referenced in this paper. It is reasonable, therefore, to neglect the kinetic energy effects as a first-order approximation, as we have done in this paper. We note, however, that material-dependent variations (either in the solid or the projectile) may be important. Molecular dynamics simulations of the impact of a single neutral argon atom with a kinetic energy of 1 keV have shown that hundreds of atoms may be dislodged from volatile (weakly bound) surfaces consisting of a cryogenically condensed gas.[62] Simulations of experiments with massive energetic projectiles such as bucky balls[63] impinging on silicon, or multiply charged fast proteins[64] impinging on biomolecular surfaces can also cause massive disruptions. Very recent studies of mica surfaces suggest that very high kinetic energy (80 meV) low-charge ions may produce surface craters similar to those observed with slow, very highly charged ions.[65]

Another aspect of the ion-surface interaction that can influence the degree to which our assumed initial conditions are realistic is the fraction of the ion's internal energy that is neutralized (a) during its approach to the surface, (b) during impact, and (c) subsequent to impact. Much work is still required to fully understand each of these three phases and, in particular, the relevant time scales that govern processes within each of them.

In addition to the limitations mentioned above, this work does not include heat conduction due to the electronic degree of freedom. We consider the amount of energy (heat) carried by the electrons as secondary compared to the overall energy redistribution. Also, the charge transfer between Si and Si$^+$ has not been considered because the time scale for charge transfer in semiconductors is much greater than the time scale of the explosion. More complete simulations of the ion-surfaced interactions are in progress.

[1] See *Materials-Fabrication and Patterning at the Nanoscale*, edited by F. Cerrina and C. R. K. Marrinan, MRS Symposia Proceedings No. 380 (Materials Research Society, Pittsburgh, 1995).

[2] See review by H. Gleiter, Nanostruct. Mater. **1**, 1 (1992), and references therein.

[3] See *Physics and Chemistry of Finite Systems: From Clusters to Crystals*, edited by P. Jena, S. N. Khanna, and B. K. Rao, Vol. 374 of *NATO Advanced Studies Institute Series C: Mathematical and Physical Sciences* (Kluwer, Dordrecht, 1992).

[4] R. T. Bate, Nanotechnology **1**, 1 (1990).

[5] H. I. Smith and H. G. Craighead, Phys. Today **43**(2), 24 (1990).

[6] J. I. Brauman *et al.*, Science **254**, 1277 (1991), special issue on Cluster.

[7] R. L. Whetten, J. T. Khoury, M. M. Alvarez, S. Murphy, I. Vesmar, Z. L. Wang, C. Cleveland, W. D. Ludtke, and Uzi Landman, Adv. Mater. **8**, 428 (1996).

[8] S. T. DeZwart, T. Fried, D. O. Boerma, R. Hoekstra, A. G. Drentje, and A. L. Boers, Surf. Sci. **177**, L939 (1986).

[9] T. Ogawa and T. Abe, J. Mat. Sci. **26**, 1903 (1991).

[10] D. Schneider, M. A. Briere, M. W. Clark, J. McDonald, J. Biersack, and W. Siekhaus, Surf. Sci. **294**, 403 (1993).

[11] Proceedings of the 29th International Conference on Electron, Ion, and Photon Beam Technology and Nanofabrication [J. Vac. Sci. Technol. B **13**, No. 6 (1995)].

[12] Proceedings of the 8th International MicroProcess Conference [Jpn. J. Appl. Phys. **34**, No. 12B, (1995)].

[13] Micro- and Nano-Engineering 95 [Microelectronic Engineering **30**, No. 1–4 (1996)].

[14] R. W. Schmieder and R. Bastasz, Proceedings of the VIth International Conference on the Physics of Highly Charged Ions, AIP Conf. Proc. No. 274 (AIP, New York, 1992), p. 690.

[15] H.-P. Cheng and Uzi Landman, Science **260**, 1304 (1993).

[16] R. N. Barnett, H.-P. Cheng, H. Hakkinen, and Uzi Landman, J. Phys. Chem. **99**, 7731 (1995).

[17] J. I. Pascual, J. Mendez, J. Gomez-Herrero, A. M. Baro, N. Garcia, Uzi Landman, W. D. Luedtke, E. N. Bogacheck, and H.-P. Cheng, Science **267**, 1793 (1995).

[18] R. S. Berry, T. L. Beck, H. L. Davis, and J. Jellinek, in Evolution of Size Effects in Chemical Dynamics, Part 2, edited by I. Prigogine and S. A. Rise [Adv. Chem. Phys. **70**, 75 (1988)].

[19] See review by U. Landman and W. D. Ludtke, Appl. Surf. Sci. **60/61**, 1 (1992). See *Clusters and Fullerences*, edited by E. Tosatti, V. J. Kumar, and T. P. Martin (World Scientific, London, 1992).

[20] See review by F. F. Abraham, Adv. Phys. **35**, 1 (1986); see also *Melting, Localization and Chaos*, edited by R. K. Kalia and P. Vashishta (Elsevier Science, Amsterdam, 1982).

[21] See *Computations for the Nanoscale*, edited by P. E. Blochl, A. J. Fisher, and C. Joachim (Kluwer, Dordrecht, 1993).

[22] R. Car and M. Parrinello, Phys. Rev. Lett. **60**, 204 (1988).

[23] H.-P. Cheng, R. N. Barnett, and Uzi Landman, Chem. Phys. Lett. **237**, 161 (1995).

[24] W. S. Warren, H. Rabitz, and M. Dahled, Science **259**, 1581 (1993).

[25] B. Kohler, J. L. Krause, F. Raksi, K. R. Wilson, V. Y. Yakovlev,

R. M. Whitmell, and Y. Yan, Accts. Chem. Res. **28**, 133 (1995).

[26] D. H. Schneider, M. A. Briere, J. McDonald, and J. Biersack, Radiat. Eff. Def. Solids **127**, 113 (1993).

[27] D. H. G. Schneider and M. A. Briere, Phys. Scr. **53**, 228 (1996).

[28] D. Schneider, M. W. Clark, B. M. Penetrante, J. McDonald, D. Dewitt, and J. N. Bardsley, Phys. Rev. A **44**, 3119 (1991).

[29] D. Schneider, D. DeWitt, M. W. Clark, R. Schuch, C. L. Cocke, R. Schmieder, K. J. Reed, M. H. Chen, R. E. Marrs, M. Levine, and R. Fortner, Phys. Rev. A **42**, 3889 (1990).

[30] J. D. Gillaspy, Y. Agilitskiy, E. W. Bell, C. M. Brown, C. T. Chantler, R. D. Daslettes, U. Feldman, L. T. Hudson, J. M. Laming, E. S. Meyer, C. A. Morgan, A. L. Pikin, J. R. Roberts, L. P. Ratliff, F. G. Serpa, J. Surga, and E. Takas, Phys. Scr. **T59**, 392 (1995).

[31] R. W. Schmieder and R. J. Bastasz (unpublished).

[32] R. W. Schmieder and R. J. Bastasz, in *Proceedings of the VIth International Conference on the Physics Highly Charged Ions* (Ref. 14), p. 675.

[33] R. Morgenstern and J. Das, Europhys. News **25**, 3 (1994).

[34] J. Limburg, J. Das, S. Schippers, R. Hoekstra, and R. Morgenstern, Phys. Rev. Lett. **73**, 786 (1994).

[35] I. Hughes, Physics World **8**, 43 (1995).

[36] N. Itabashi, K. Mochiji, H. Shimizu, S. Ohtani, Y. Kato, H. Tanuma, N. Kobayashi, Jpn. J. Appl. Phys. **34**, 6861 (1995).

[37] I. S. Bitenskii, M. N. Murakhmetov, and E. S. Parilis Zh. Tekh. Fiz. **49**, 1044 (1979) [Sov. Phys. Tech. Phys. **24**, 618 (1979)].

[38] M. A. Briere, T. Schnekel, and D. Schneider (unpublished).

[39] P. Apell, Nucl. Instrum. Methods B **23**, 242 (1987).

[40] J. P. Briand, L. de Billy, P. Charles, S. Essabaa, P. Briand, R. Geller, J. P. Desclaux, S. Bliman, and C. Ristori, Phys. Rev. Lett. **65**, 159 (1990).

[41] J. P. Briand, B. d'Etat, D. Schneider, M. Clark, and V. Decaux, Nucl. Instrum. Methods B **87**, 138 (1994).

[42] B. d'Etat, J. P. Briand, G. Ban, L. de Billy, J. P. Desclaux, and P. Briand, Phys. Rev. A **48**, 1098 (1993).

[43] J.-P. Briand, B. d'Etat-Ban, D. Schneider, M. A. Briere, V. Decaux, J. W. McDonald, and S. Bardin, Phys. Rev. A **53**, 2194 (1996).

[44] F. Aumayr, H. Kurz, D. Schneider, M. A. Briere, J. W. McDonald, C. E. Cunningham, and H. P. Winter, Phys. Rev. Lett. **71**, 1943 (1993).

[45] P. Apell, J. Phys. B **21**, 2665 (1988).

[46] J. N. Bardsley and B. M. Penetrante, Comments At. Mol. Phys. **27**, 43 (1991).

[47] E. Y. Wu, R. J. Friauf, and T. P. Armstrong, Surf. Sci. **249**, 350 (1991).

[48] N. Vaeck and J. E. Hansen, J. Phys. B **28**, 3523 (1995).

[49] J. Tersoff, Phys. Rev. B **39**, 5566 (1988).

[50] S. Wei (private communication).

[51] M. P. Allen and D. J. Tildesley, *Computer Simulations of Liquids* (Clarendon, Oxford, United Kingdom, 1987).

[52] K. Y. Kim, W. Sachse, and A. G. Every, J. Acoust. Soc. Am. **93**, 1393 (1993).

[53] K. M. Yoo, X. M. Zhao, M. Siddique, R. R. Alfano, D. P. Osterman, M. Radparvat, and J. Cunniff, in *Chemical Physics*, edited by C. B. Harris, E. P. Ippen, G. A. Morou, and A. H. Zewail (Springer-Verlag, 1990), Vol. 53, p. 357.

[54] P. B. Allen, Phys. Rev. Lett. **59**, 1460 (1987); S. D. Broson, J. G. Fujimoto, and E. P. Ippen, Phys. Rev. Lett. **59**, 1962 (1987).

[55] D. C. Parks, R. Bastasz, R. W. Schmieder, and M. Stockli, J. Vac. Sci. Technol. B **13**, 941 (1995).

[56] J. Burgodorfer, C. Reinhold, L. Hagg, and F. Meyer, Aust. J. Phys. **49**, 527 (1996).

[57] L. Folkerts, S. Schippers, D. M. Zehner, and F. W. Meyer, Phys. Rev. Lett. **74**, 2204 (1995).

[58] P. Barga, Comments At. Mol. Phys. **23**, 111 (1989).

[59] N. Stolterfoht, A. Arnau, M. Grether, R. Kohrbruck, A. Spieler, R. Page, A. Saal, J. Thomaschewski, and J. Bleck-Neuhaus, Phys. Rev. A **52**, 445 (1995).

[60] S. Schippers, S. Hustedt, W. Heiland, R. Kohrbruck, J. Bleck-Neuhaus, J. Kemmler, D. Leeler, N. Stolterfoht, Nucl. Instrum. Methods B **78**, 106 (1993).

[61] X.-S. Wang, R. J. Pechman, and J. H. Weaver, J. Vac. Sci. Technol. B **13**, 2031 (1995).

[62] H. Urbassek and K. T. Waldeer, Phys. Rev. Lett. **67**, 105 (1991).

[63] R. Smith, K. Beardmore, and A. Gras-Marti, Vacuum **46**, 1195 (1995).

[64] C. T. Reimann, A. P. Quist, J. Kopniczky, B. U. R. Sundqvist, R. Erlandsson, and P. Tengvall, Nucl. Instrum. Methods B **88**, 29 (1994).

[65] D. D. N. Barlo Daya, A. Hallen, P. Hakansson, B. U. R. Sundqvist, and C. T. Reimann, Nucl. Instrum. Methods B **103**, 454 (1995).